Theoretical analysis on the possibility of superconductivity in the trilayer Ruddlesden-Popper nickelate $La_4Ni_3O_{10}$ under pressure and its experimental examination: Comparison with $La_3Ni_2O_7$

Hirofumi Sakakibara[1,*], Masayuki Ochi[2,3,*], Hibiki Nagata,[4,5,*] Yuta Ueki,[4,5,*] Hiroya Sakurai[4,*], Ryo Matsumoto,[4]
Kensei Terashima,[4] Keisuke Hirose,[6] Hiroto Ohta[6], Masaki Kato,[6] Yoshihiko Takano[4,5,†] and Kazuhiko Kuroki[2,‡]

[1]*Advanced Mechanical and Electronic System Research Center(AMES), Faculty of Engineering,*
Tottori University, 4-10 Koyama-cho, Tottori, Tottori 680-8552, Japan
[2]*Department of Physics, Osaka University, 1-1 Machikaneyama-cho, Toyonaka, Osaka 560-0043, Japan*
[3]*Forefront Research Center, Osaka University, 1-1 Machikaneyama-cho, Toyonaka, Osaka 560-0043, Japan*
[4]*MANA, National Institute for Materials Science (NIMS), 1-2-1 Sengen, Tsukuba 305-0047, Japan*
[5]*Graduate School of Science and Technology, University of Tsukuba, 1-1-1 Tennodai, Tsukuba, Ibaraki 305-8577, Japan*
[6]*Department of Molecular Chemistry and Biochemistry, Doshisha University, 1-3 Tataramiyakotani, Kyo-Tanabe 610-0321, Japan*

We study the possibility of superconductivity in a trilayer Ruddlesden-Popper nickelate $La_4Ni_3O_{10}$ under pressure both theoretically and experimentally, making comparison with the recently discovered high T_c superconductor $La_3Ni_2O_7$, a bilayer nickelate. Through DFT calculations, we find that a structural phase transition from monoclinic to tetragonal takes place around 10–15 GPa. Using the tetragonal crystal structure, we theoretically investigate the possibility of superconductivity, where a combination of fluctuation exchange approximation and linearized Eliashberg equation is applied to a six-orbital model constructed from first-principles band calculations. The obtained results suggests that $La_4Ni_3O_{10}$ may also become superconducting under high pressure with T_c comparable to some cuprates, although it is not as high as $La_3Ni_2O_7$. We also perform experimental studies using our polycrystalline samples of $La_3Ni_2O_{7.01}$ and $La_4Ni_3O_{9.99}$. The superconducting transition of $La_3Ni_2O_{7.01}$, with a maximum onset T_c of 67.0 K at a pressure of 26.5 GPa, is confirmed by a drop in the electrical resistance as well as the magnetic-field dependence of the resistance. Quite interestingly, similar temperature and magnetic field dependencies of the resistance are also observed for $La_4Ni_3O_{9.99}$, where a drop in the resistance is observed at lower temperatures compared to $La_3Ni_2O_{7.01}$, under pressures of 32.8 GPa and above. Given the theoretical expectation, the reduction in the resistance can most likely be attributed to the occurrence of superconductivity in $La_4Ni_3O_{9.99}$. The temperature at which the resistance deviates from linear behavior, considered as the onset T_c, monotonically increases up to 23 K at 79.2 GPa, which is opposite to the pressure dependence of T_c in $La_3Ni_2O_{7.01}$.

I. INTRODUCTION

Even vs odd number effects have often been issues of interest in various fields of physics. A famous example in condensed matter physics is Haldane's conjecture, which states that in a spin-$N/2$ antiferromagnetic Heisenberg chain, the excitation spectrum is gapless and the spin-spin correlation exhibits a slow (algebraic) decay when N is an odd number, whereas when N is even, there is a gap in the excitation and the spin correlation decays exponentially [1]. Schulz discussed the relation between a spin-$N/2$ antiferromagnetic Heisenberg chain and N coupled spin-1/2 chains [2,3], namely, N-leg ladders, and argued that when N is even, the system is gapfull, while the system becomes gapless when N is odd. In the 1990s, following the studies by Dagotto *et al.* [4] and Rice *et al.* [5], spin-1/2 antiferromagnetic N-leg ladders were

intensively studied both theoretically and experimentally [6]. Due to the opening of the spin gap in the case of $N =$ even, the possibility of superconductivity in doped even-leg (two-leg, in particular) Hubbard and t-J models was widely investigated both analytically and numerically [4–6]. Indeed, a cuprate that contains two-leg ladders was found to superconduct under pressure [7].

Here, an interesting problem arises regarding the possibility of superconductivity in doped *odd*-number-leg ladders. One might expect an absence of superconductivity due to the absence of the spin gap, but one of the present authors and his colleagues showed that superconductivity can still take place in the three-leg Hubbard ladder [8] based on the weak coupling analysis that shows two out of three spin modes are gapped [9,10]. A similar result was also obtained in Ref. [3], and the weak coupling analysis was soon extended to N-leg ladders [11].

A two-dimensional analog of the two-leg ladder model, namely, the bilayer model, typically on a square lattice, has also been a target of theoretical interest from the perspective of unconventional superconductivity. When two square

*These authors contributed equally to this work.
†TAKANO.Yoshihiko@nims.go.jp
‡kuroki@presto.phys.sci.osaka-u.ac.jp

lattices are coupled by a large vertical hopping $t_\perp$ or a strong vertical magnetic coupling $J_\perp$, opening of a spin gap is expected, and various studies have shown strong enhancement of interlayer pairing superconductivity [4,12–20]. Motivated by the very strong enhancement of superconductivity near half filling found in some studies [13,14], one of the present authors investigated the possibility of realizing the bilayer Hubbard model with large $t_\perp$ in actual materials, and ended up with a bilayer Ruddlesden-Popper nickelate $La_3Ni_2O_7$ [16]. The key factor there was that the Ni $3d_{3z^2-r^2}$ orbitals, which are elongated in the out-of-plane direction and hence enhance $t_\perp$, are close to half filling in this material. Quite recently, superconductivity in $La_3Ni_2O_7$ with a maximum T_c of 80 K has been discovered under high pressure [21], which has sparked a vast wave of interest both experimentally [22–25] and theoretically [26–54], including ours [55].

Given the recent developments in bilayer $La_3Ni_2O_7$, and also the previous studies regarding even vs odd-leg ladders as described above, it is natural to consider investigating the possibility of superconductivity in a trilayer Ruddlesden-Popper nickelate $La_4Ni_3O_{10}$. Since $La_4Ni_3O_{10}$ is not superconducting at ambient pressure, we will consider its possibility under pressure as in $La_3Ni_2O_7$ both theoretically and experimentally. Since superconductivity in $La_3Ni_2O_7$ appears to occur when the symmetry of the crystal structure becomes (close to) tetragonal under high pressure [21], we first investigate theoretically whether the crystallographic symmetry of $La_4Ni_3O_{10}$ becomes tetragonal under high pressure. Indeed, we find that a structural phase transition from monoclinic to tetragonal takes place around 10–15 GPa. Adopting a hypothesis that superconductivity in $La_4Ni_3O_{10}$, if any, occurs when the crystallographic symmetry is tetragonal, we investigate the possibility of superconductivity using the crystal structure obtained at 40 GPa, which is safely in the tetragonal phase regime. A combination of fluctuation exchange approximation (FLEX) and linearized Eliashberg equation is applied to a six-orbital (2 orbitals ×3 layers) model constructed from first-principles band calculations. Our calculation results suggest that $La_4Ni_3O_{10}$ may also become superconducting under high pressure with T_c comparable to some cuprates, although it is not as high as $La_3Ni_2O_7$.

We also present experimental results for our polycrystalline samples of $La_3Ni_2O_{7.01}$ and $La_4Ni_3O_{9.99}$. The superconducting transition of $La_3Ni_2O_{7.01}$, with a maximum onset T_c of 67.0 K at a pressure of 26.5 GPa, is confirmed by a drop in the electrical resistance, as well as the magnetic field dependence of the resistance. Quite interestingly, similar temperature and magnetic field dependencies of the resistance are observed also for $La_4Ni_3O_{9.99}$, where a drop in the resistance is observed at lower temperatures compared to $La_3Ni_2O_{7.01}$, under pressures of 32.8 GPa and above. Given the theoretical expectation, the reduction in the resistance can most likely be attributed to the occurrence of superconductivity in $La_4Ni_3O_{9.99}$.

II. THEORETICAL METHOD

For density functional theory (DFT) calculation, we use the PBEsol exchange-correlation functional [56] and the projector augmented wave method (PAW) [57] as implemented in the VIENNA AB INITIO SIMULATION PACKAGE (VASP) [58–61]. Core-electron states in PAW potentials are [Kr]$4d^{10}$, [Ar], and [He] for La, Ni, and O, respectively. We use a plane-wave cutoff energy of 600 eV for Kohn-Sham orbitals without including the spin-orbit coupling for simplicity.

We perform structural optimization until the Hellmann-Feynman force becomes less than 0.01 eV Å^{-1} for each atom using an $8 \times 8 \times 2$ $\mathbf{k}$-mesh. To verify the stability of the optimized crystal structure under pressure, we calculate the phonon dispersion using the finite displacement method as implemented in the PHONOPY [62] software in combination with VASP. We use a $3 \times 3 \times 1$ $\mathbf{q}$-mesh for a conventional tetragonal unit cell containing 34 atoms. For a $3 \times 3 \times 1$ supercell used for finite-displacement calculations, we use a $4 \times 4 \times 2$ $\mathbf{k}$-mesh.

To discuss superconductivity, we extract Ni-$d_{x^2-y^2}$ and $d_{3z^2-r^2}$ Wannier orbitals using WANNIER90 software [63–65]. For this purpose, we use the tetragonal crystal structure under the pressure of 40 GPa obtained by our calculation. We use an $12 \times 12 \times 12$ $\mathbf{k}$-mesh for a primitive unit cell. We adopt FLEX [66,67] to take into account the effect of electron correlation as in Ref. [55] for $La_3Ni_2O_7$. As for the interaction term of the Hamiltonian, we take the on-site interactions, namely, intraorbital (interorbital) Coulomb interactions $U(U')$, Hund's coupling J, and pair hopping J'. We assume the orbital rotational symmetry and take the same value of U for the $d_{x^2-y^2}$ and $d_{3z^2-r^2}$ orbitals, and $U' = U - 2J, J = J'$. As a typical value of the interactions, we take $U = 3$ eV, $J = J' = 0.3$ eV, and $U' = U - 2J = 2.4$ eV. These interaction values are the same as those adopted in our study for $La_3Ni_2O_7$, which can be considered as typical values for $3d$-transition-metal oxides [68]. We calculate the self-energy induced by the spin-fluctuation formulated as shown in the literature [69–71] in a self-consistent calculation. The real part of the self-energy at the lowest Matsubara frequency is subtracted in the same manner with Ref. [72] to maintain the band structure around the Fermi level obtained by first-principles calculation.

We use the linearized Eliashberg equation to study the possibility of superconductivity, also as in Ref. [55] for $La_3Ni_2O_7$. The renormalized Green's functions obtained by FLEX are plugged into this equation. Also, the pairing interaction kernel in this equation is obtained from the FLEX Green's function as a purely electronic one (i.e., phonon-mediated pairing interaction is not considered), which is mainly dominated by spin fluctuations in the present case. Since the the eigenvalue λ of the Eliashberg equation monotonically increases upon lowering the temperature, and reaches unity at $T = T_c$, we adopt λ calculated at a fixed temperature, $T = 0.01$ eV as a measure of superconductivity. For convenience, we will call the eigenfunction (with the largest eigenvalue) of the linearized Eliashberg equation at the lowest Matsubara frequency $i\omega(= i\pi k_B T)$, the superconducting gap function. We take a $16 \times 16 \times 4$ k-point mesh and 2048 Matsubara frequencies for the FLEX calculation.

III. EXPERIMENTAL METHOD

Polycrystalline samples of $La_3Ni_2O_{7.01}$ and $La_4Ni_3O_{9.99}$ were employed for electrical resistance measurements

under high-pressure conditions. Polycrystalline samples of $La_3Ni_2O_7$ and $La_4Ni_3O_{10}$ were prepared using a conventional solid-state reaction with La_2O_3 and NiO. The raw materials were stoichiometrically mixed, pressed into pellets, and heated at $1000\,°C$ for 12 h in flowing oxygen. Subsequently, the pellets were crushed, repelletized, and fired at $1300\,°C$ for the former sample and $1200\,°C$ for the latter, each for 12 h in flowing oxygen. Repeating the same heat treatment led to the formation of almost single-phase samples. Further processes were implemented to enhance homogeneity and minimize crystal defects. Specifically, the samples were initially reduced by hydrogen to decompose them into La_2O_3 and Ni metal. The samples were then subjected to two additional heating cycles at the target temperatures of $1300\,°C$ or $1200\,°C$ for 12 h in flowing oxygen, with intermediate grinding. A similar method was reported for $Y_2Ba_4Cu_7O_{15-\delta}$ to eliminate stacking faults [73]. Following the final firing, the samples underwent a slow cooling process to $1000\,°C$ for 3 h, $500\,°C$ for 12 h, and room temperature for approximately 8 h. This aimed to uniformly increase oxygen content and reduce potential crystal defects. The oxygen contents at this stage were estimated to be 7.01 for the former sample and 9.89 for the latter by using a method detailed later.

The $La_4Ni_3O_{10}$ sample underwent annealing in high oxygen pressure to increase its oxygen content via hot isostatic pressing, utilizing a commercial system (O_2-Dr.HIP, Kobelco). The sample was placed in the system and heated at $600\,°C$ under $1500\ kgf/cm^2$ of 20% O_2/Ar for 2 h. The oxygen content after the HIP treatment was estimated to be 9.99.

The final products were characterized by powder x-ray diffraction (XRD) from $2\theta = 5° - 80°$ with Cu K_α radiation using a commercial diffractometer of MiniFlex600 (Rigaku) equipped with a high-speed one-dimensional detector, D/teX Ultra. The lattice parameters were estimated, assuming the orthorhombic structure reported previously [74], to be $a = 5.3903(9)\text{Å}$, $b = 5.4464(7)\text{Å}$, $c = 20.507(5)\text{Å}$ for $La_3Ni_2O_{7.01}$, and $a = 5.411(6)\text{Å}$, $b = 5.463(6)\text{Å}$, $c = 27.98(3)\text{Å}$ for $La_4Ni_3O_{9.99}$. As shown in Fig. 1, XRD patterns indicate single-phase samples with sharp peaks and no discernible stacking faults or defects. Interestingly, $La_4Ni_3O_{10}$ sample was partially decomposed into $La_3Ni_2O_7$ and NiO at $1300\,°C$ in 1 atm oxygen gas, whereas $La_3Ni_2O_7$ sample was observed to partially decompose into $La_4Ni_3O_{10}$ and La_2O_3 at $1200\,°C$ under $2000\ kgf/cm^2$ of 20% O_2/Ar [75]. These phase relations, as well as adopting the hydrogen reduction process, strongly suggest that our final products do not include an influential amount of stacking faults in the appearance of the superconductivity shown below.

Oxygen contents were estimated through weight change via hydrogen reduction, a method commonly employed in literature. A sample was placed in a gold crucible and heated at $800\,°C$ for 12 h in a furnace connected to a glove box filled with argon gas. The reduced sample was transferred directly into the glove box without exposure to air to prevent water absorption by La_2O_3, and its weight was measured. To ensure accuracy, over 0.3 g of the sample was used, and the weight was measured with a precision of 10^{-5} g using a high-spec balance (XP205DR, Mettler Toledo). Each weight was determined through at least three measurements, with
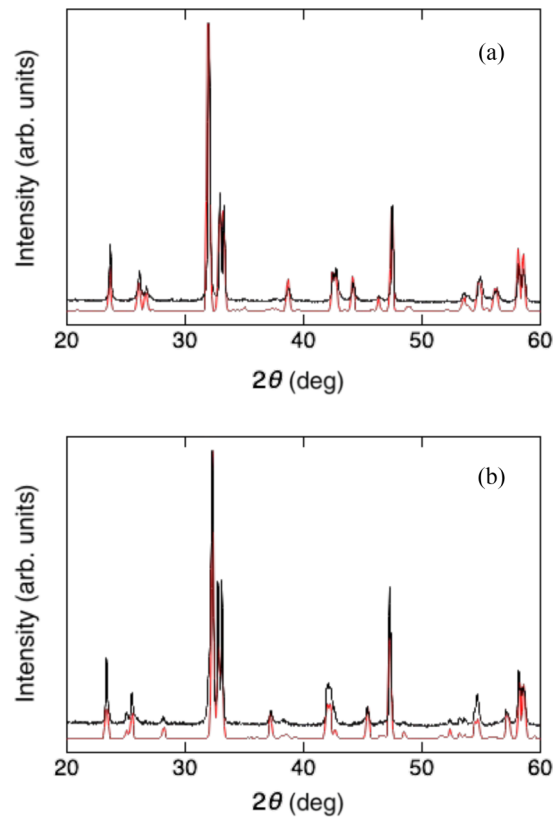

FIG. 1. Powder x-ray diffraction patterns of $La_3Ni_2O_{7.01}$ (a) and $La_4Ni_3O_{9.99}$ (b). The red lines are the simulated patterns for the crystal structures reported for each compound [74].

differences no greater than 1×10^{-5} g between them. More details of sample preparation and characterization will be published elsewhere [75].

High pressure was generated with diamond anvil cell (DAC) with boron-doped diamond electrodes designed for four-terminal resistance measurement [76,77]. Cubic boron nitride powder was used as a pressure-transmitting medium. Applied pressure was estimated by fluorescence of ruby placed near the sample up to 20 GPa [78]. For pressure beyond 20 GPa, applied pressure was estimated by a Raman spectrum from a culet of the top diamond anvil obtained by Raman Microscope (Renishaw) [79]. Details of the cell configuration will be described in the literature [80,81]. Temperature and magnetic fields were controlled by PPMS (Quantum Design).

IV. THEORETICAL RESULTS–CRYSTAL STRUCTURE

We optimized the crystal structure under pressure by DFT calculations. Here, we note that several different space groups have been reported in literature for $La_4Ni_3O_{10}$ at ambient pressure, $Fmmm$ [83] (or $Imm2$ considering a symmetry lowering mentioned in this paper, as pointed out in Ref. [84]), $Cmce$ ($Bmab$) [74,84,85], $P2_1/a$ ($Z = 4$) (i.e., $P2_1/a$ containing four formula units in the unit cell) [86–88] as was also reported for $Nd_4Ni_3O_{10-\delta}$ [89,90], and $P2_1/a$ ($Z = 2$) [84,91] as was also reported for $Pr_4Ni_3O_{10}$ [92]. It was pointed out that samples were mixed phases of orthorhombic and monoclinic symmetry [84,93]. The stability of several phases,
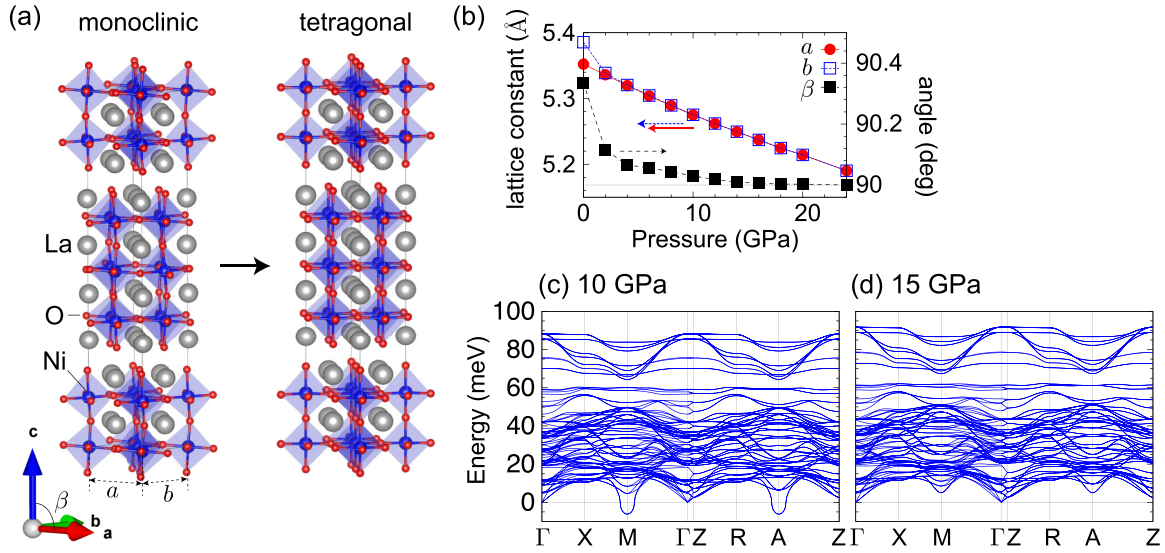
FIG. 2. (a) Optimized crystal structures of $La_4Ni_3O_{10}$ in the monoclinic and tetragonal phases. Gray, blue, and red spheres denote La, Ni, and O atoms, respectively. Crystal structure was depicted using VESTA software [82]. (b) Lattice parameters a, b, and β obtained by structural optimization with the $P2_1/a$ ($Z = 4$) space group under pressure. (c), (d) Phonon dispersion of the tetragonal $I4/mmm$ structure under the pressure of 10 and 15 GPa, respectively.

Cmce, *Pbca*, and two types of $P2_1/a$, was also investigated by DFT calculation [94]. Due to the complexity of the situation, we first optimized a crystal structure under pressure assuming a monoclinic space group of $P2_1/a$ ($Z = 4$), which has a relatively low symmetry among these candidates and is a subgroup of some of the candidates, and next checked the stability of the obtained structure under pressure by phonon calculation.

By the structural optimization of a $P2_1/a$ ($Z = 4$) structure under pressure, we found that the structural phase transition from monoclinic to tetragonal takes place as shown in Fig. 2(a). In fact, lattice parameters relevant to the monoclinic-tetragonal transition, a, b, and β, were shown in Fig. 2(b), where $a = b$ and $\beta = 90°$ were realized around 10–15 GPa. We also confirmed that the obtained tetragonal structure belongs to the $I4/mmm$ space group by checking atomic coordinates. Then, we performed phonon calculation for the tetragonal $I4/mmm$ structure under the pressure of 10 and 15 GPa as shown in Figs. 2(c)–2(d). While the calculated phonon dispersion has an imaginary mode at 10 GPa, this instability disappears at 15 GPa, by which we confirmed that the structural transition takes place around 10–15 GPa and the tetragonal structure is dynamically stable above 15 GPa. Our calculation shows that several tens of gigapascal pressure gives rise to a tetragonal structure, as in $La_3Ni_2O_7$ [21].

V. THEORETICAL RESULTS—BAND STRUCTURE AND SUPERCONDUCTIVITY

We now study the possibility of superconductivity in the tetragonal phase, which can be considered natural due to the enhanced electronic hopping between the layers, which is likely to favor interlayer pairing superconductivity, as in $La_3Ni_2O_7$. In Fig. 3(b), we present the band structure of

the six-orbital model of $La_4Ni_3O_{10}$ at 40 GPa. Some of the key parameter values are listed in Table I. For comparison, in Fig. 3(a), we also show the band structure of the four-orbital model of $La_3Ni_2O_7$ obtained in our previous study [55]. While there are bonding (colored blue) and antibonding (green) $d_{3z^2-r^2}$ bands in $La_3Ni_2O_7$, in $La_4Ni_3O_{10}$, there is an additional nonbonding $d_{3z^2-r^2}$ band (yellow) between the bonding and antibonding bands [98,99]. Interestingly, the Fermi level in $La_4Ni_3O_{10}$ is placed near the top of the bonding $d_{3z^2-r^2}$ band, while the bottom of the antibonding band is placed somewhat above the Fermi level, which is a situation similar to that in $La_3Ni_2O_7$. This similarity occurs due to a combination of two discrepancies between these materials, namely, (i) there is a nonbonding $d_{3z^2-r^2}$ band in $La_4Ni_3O_{10}$ and (ii) the formal Ni valence is $+2.67$ in $La_4Ni_3O_{10}$ against $+2.5$ in $La_3Ni_2O_7$.

Let us now see how this similarity and discrepancies of the band structure between the two materials is reflected in

TABLE I. The orbital level offset $\Delta E = E_{x^2-y^2} - E_{3z^2-r^2}$ between $d_{x^2-y^2}$ and $d_{3z^2-r^2}$ orbitals, the vertical interlayer hopping $t_\perp$ between the $d_{3z^2-r^2}$ orbitals, the nearest-neighbor intralayer hoppings $t_{3z^2-r^2}$, $t_{x^2-y^2}$, and $t_{x^2-y^2-3z^2-r^2}$ of $La_4Ni_3O_{10}$ are displayed. Parameters (except for $t_\perp$) for the inner- and outer-layers are shown in the second and third rows, respectively. Here, the onsite energy of the inner-layer $d_{x^2-y^2}$ ($d_{3z^2-r^2}$) orbitals is 0.264 eV (0.416 eV) higher than that for the outer layer. The parameters of $La_3Ni_2O_7$ presented in Ref. [55] are also displayed in the lowest row for comparison.

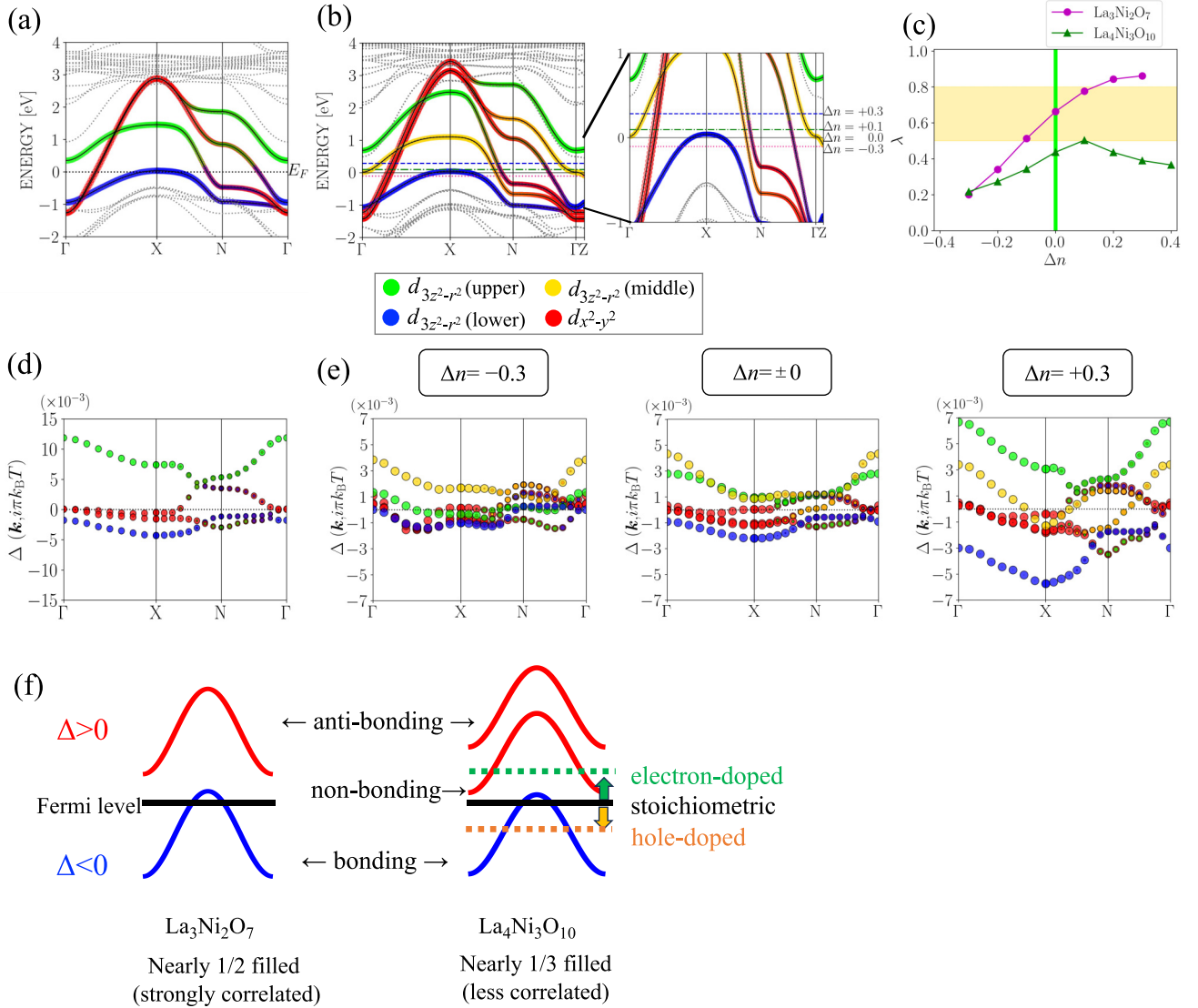| (eV)	ΔE	$t_\perp$	$t_{3z^2-r^2}$	$t_{x^2-y^2}$	$t_{x^2-y^2-3z^2-r^2}$
Inner	0.102		-0.163	-0.543	-0.297
Outer	0.255	-0.715	-0.148	-0.539	-0.285
$La_3Ni_2O_7$	0.372	-0.664	-0.117	-0.491	-0.242

FIG. 3. (a) The band structure of the four-orbital model of $La_3Ni_2O_7$ [55]. (b) The band structure of the six-orbital model of $La_4Ni_3O_{10}$. On the right is a blowup near the Fermi level, together with the Fermi level for various band fillings. (c) The eigenvalue of the Eliashberg equation for $La_4Ni_3O_{10}$ and $La_3Ni_2O_7$ [55] plotted against the band filling measured from stoichiometry. The yellow hatched region indicates the range of λ obtained by the same method for various cuprates [95–97]. (d) Superconducting gap functions of $La_3Ni_2O_7$ for $\Delta n = 0$ [55]. (e) Superconducting gap functions of $La_4Ni_3O_{10}$ for $\Delta n = -0.3$ (left), $\Delta n = 0$ (center), $\Delta n = +0.3$ (right). (f) Schematic picture of the superconducting gap functions of $La_3Ni_2O_7$ and $La_4Ni_3O_{10}$. The strength of Wannier orbital characters are presented in (a), (b), (d), (e) with the thickness and radius of the color coded line and circles, where the "sum" of the $d_{x^2-y^2}(d_{3z^2-r^2})$ orbital characters among inner and outer layers are indicated by red (green, blue, and yellow). The yellow color is used for indicating the $d_{3z^2-r^2}$ characters in the case that the eigenstate contains the inner-layer components less than 5%. Otherwise, either green or blue is used for the $d_{3z^2-r^2}$ components, depending on whether the band energy is above or below 0.2 eV. In this way, the colors blue, yellow, and green represent bonding, nonbonding, and antibonding $d_{3z^2-r^2}$ bands, respectively. All the calculation results for $La_4Ni_3O_{10}$ are obtained using the crystal structure at 40 GPa.

superconductivity. In Fig. 3(c), the eigenvalue of the Eliashberg equation λ of the six-orbital model of $La_4Ni_3O_{10}$ is plotted against the band filling (defined as the number of electrons per unit cell per spin), which is measured from that of the stoichiometric composition (two electrons). For comparison, we plot λ for the four-orbital model of $La_3Ni_2O_7$ [55]. The eigenvalue is found to be smaller for $La_4Ni_3O_{10}$ than for $La_3Ni_2O_7$, but a notable difference regarding the band-filling dependence is that while λ monotonically decreases for $La_3Ni_2O_7$ when the band filling is decreased, namely, when it

moves away from half filling, for $La_4Ni_3O_{10}$, λ is (locally) maximized near the stoichiometric composition. Consequently, its value (0.433) for $La_4Ni_3O_{10}$ at stoichiometry is not small, in the sense that it is still comparable to those of some of the cuprates (with relatively low T_c) obtained by the same method [95–97]. The relatively small reduction of λ compared to that of $La_3Ni_2O_7$ is even more interesting considering the fact that the band filling of the $d_{3z^2-r^2}$ orbitals in $La_4Ni_3O_{10}$ is only roughly 1/3 (per Ni atom per spin), compared to roughly 1/2 (half filling) in $La_3Ni_2O_7$, so the electron correlation

effects are expected to be significantly smaller in the former.

To understand the origin of the band-filling dependence of λ, we plot in Fig. 3(e) the superconducting gap function of the model of $La_4Ni_3O_{10}$ for various band fillings, together with that of $La_3Ni_2O_7$ (at stoichiometry) obtained in Ref. [55] [Fig. 3(d)]. At stoichiometry in $La_4Ni_3O_{10}$, the sign of the gap is reversed not only between bonding and antibonding $d_{3z^2-r^2}$ bands (as in $La_3Ni_2O_7$), but also between bonding and nonbonding bands. When the band filling is decreased from stoichiometry (when holes are doped), the superconducting gap of the antibonding band becomes small, while when electrons are doped, the gap of the nonbonding band becomes small. Also, all the bands are fully gapped at stoichiometry, while the small gaps are nodal when doped. From these results, we may conclude that the (locally) maximized and relatively large λ obtained for $La_4Ni_3O_{10}$ around stoichiometry, despite $d_{3z^2-r^2}$ orbitals being away from half filling, is because all three $d_{3z^2-r^2}$ bands contribute to superconductivity. This, in turn, can be attributed to the relation between the Fermi level and the band edges; around stoichiometry, the edge of all three bands touches or lies close to the Fermi level, namely, all the bands are (nearly) incipient, which pushes up the spin fluctuations to finite energies, thereby making them more effective as pairing glue [16,100]. When holes are doped, the Fermi level moves away from the antibonding band bottom, whereas for electron doping, the Fermi level firmly intersects the nonbonding band. These situations are schematically presented in Fig. 3(f). It is also worth noting that the role played by the nonbonding band is quite different from that in the three-leg Hubbard ladder, where the nonbonding band is irrelevant for superconductivity [8]. Although the origin of this discrepancy is not clear at present, there are differences in that $t_\perp$ is much larger than the in-plane hoppings and also the band filling is far away from half filling in the present model, besides the obvious differences in the dimensionality and the presence of the inter-orbital hybridization. In the above, we have mainly focused on the gap function of the $d_{3z^2-r^2}$ orbitals, but as for the $d_{x^2-y^2}$ orbitals, the gap function takes relatively large values around the N point in all cases presented here, where the hybridization between the $d_{x^2-y^2}$ and $d_{3z^2-r^2}$ orbitals is strong. This tendency is similar to that found in our calculation for $La_3Ni_2O_7$ [55].

Finally, we study the pressure dependence of the superconductivity. We also perform similar FLEX calculations at 20 and 60 GPa and obtain the eigenvalue λ. The eigenvalue is plotted against pressure in Fig. 4, which suggests that T_c is expected to increase upon increasing the pressure.

VI. EXPERIMENTAL RESULTS—$La_3Ni_2O_{7.01}$

We now turn to the experimental results. We first focus on $La_3Ni_2O_{7.01}$. Figure 5 displays the temperature dependence of the electrical resistance under various pressures and magnetic fields. Semiconducting behavior is observed below 20.0 GPa, as shown in Fig. 5(a), although it is likely caused by extrinsic factors such as grain boundary scattering because $La_3Ni_2O_{7-\delta}$ ($\delta \sim 0$) has been reported to exhibit metallic properties under ambient pressure [101]. At 26.5 GPa, the superconducting transition with an onset T_c around 67.0 K is clearly rec-
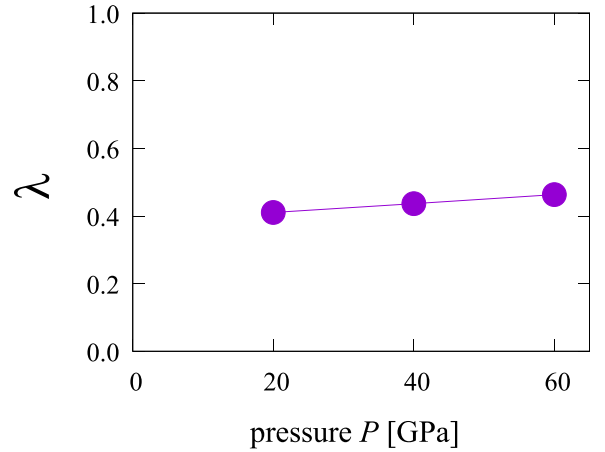

FIG. 4. The eigenvalue of the Eliashberg equation for $La_4Ni_3O_{10}$ plotted against the external pressure.

ognized, which is a behavior similar to that of $La_3Ni_2O_7$ single crystals in previous studies [21,23,24], although the amount of the resistance drop is not as significant as in those studies. T_c appears to decrease with increasing pressure as shown in Fig. 5(b). The superconductivity survives even at magnetic fields of 5 T although the resistance drop below T_c diminishes significantly with increasing field, as shown in Fig. 5(c). T_c exhibits small field dependence, i.e., 67.0 K (0 T) to 65.3 K (5 T), which is also consistent with previous studies [21,23,24].

VII. EXPERIMENTAL RESULTS–$La_4Ni_3O_{9.99}$

We now present experimental results for $La_4Ni_3O_{9.99}$. Figure 6 shows the temperature dependence of the electrical resistance under various pressures and magnetic fields. $La_4Ni_3O_{9.99}$ displays metallic behavior across all measured pressures, with a slight upturn observed at temperatures below approximately 100 K, as shown in Fig. 6(a). The origin of the upturn is uncertain at present. Intriguingly, the drop in resistance suddenly appears below 5 K at 32.8 GPa. Upon increasing the pressure beyond 46.2 GPa, the temperature at which the resistance is maximized increases and also the decrease in the resistance below it becomes more pronounced, as seen in Fig. 6(b). Here, it should be remembered that according to our theoretical calculation, the tetragonal structure is stabilized beyond pressures around 10–15 GPa in $La_4Ni_3O_{10}$, for which superconductivity with a T_c lower than that of $La_3Ni_2O_7$ is expected to take place around stoichiometric composition. Since the pressures where the reduction in the resistance is observed are well in the tetragonal phase regime, this reduction can most likely be attributed to pressure-induced superconductivity of $La_4Ni_3O_{9.99}$, although the magnitude of the resistance drop is not as significant as in single crystal $La_3Ni_2O_7$ [21,23,24], similarly to our data for polycrystalline $La_3Ni_2O_{7.01}$. In fact, the magnetic field dependence of the resistance is quite similar to that of $La_3Ni_2O_{7.01}$ as shown in Fig. 6(c), namely, the peak position of the resistance is nearly unaffected, while the resistance drop becomes less significant with increasing field. On the other hand, as seen in Fig. 6(b), the temperature at which
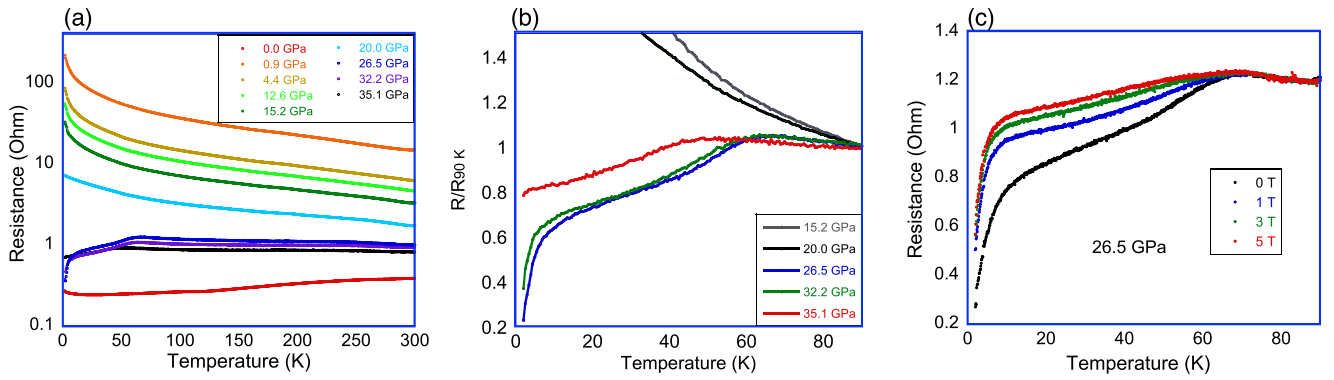
FIG. 5. Temperature dependence of the electrical resistance of $La_3Ni_2O_{7.01}$ (a) under several pressures from 0.0 GPa to 35.1 GPa, (b) normalized at 90 K under 15.2–35.1 GPa, (c) under magnetic fields from 0 to 5 T at 26.5 GPa.

the resistance deviates from a linear behavior, considered as the onset T_c, monotonically increases up to 23 K upon increasing the pressure up to 79.2 GPa, which is a pressure dependence opposite to what is observed in $La_3Ni_2O_{7.01}$ and hence is characteristic of $La_4Ni_3O_{9.99}$. This tendency may also be considered as consistent with the theoretical results, where the eigenvalue of the Eliashberg equation increases with pressure (Fig. 4).

VIII. CONCLUSION

In the present paper, we have investigated the possibility of superconductivity in $La_4Ni_3O_{10}$ under pressure both theoretically and experimentally. Through DFT calculations, we have found that a structural phase transition from monoclinic to tetragonal takes place around 10–15 GPa. Using the crystal structure obtained at 40 GPa, we have theoretically investigated the possibility of superconductivity, where a combination of FLEX and linearized Eliashberg equation is applied to a six-orbital model constructed from first-principles band calculations. An interesting feature found here is that the eigenvalue of the Eliashberg equation is (locally) maximized around stoichiometry, reflecting the fact that all three $d_{3z^2-r^2}$ bands contribute to superconductivity around this band filling.

This is due to the fact that all the bands are (nearly) incipient, which pushes up the spin fluctuations to finite energies and makes them more effective as pairing glue. Hence our calculation results suggest that $La_4Ni_3O_{10}$, around stoichiometric composition, may become superconducting under high pressure with T_c comparable to some cuprates, although it is not as high as $La_3Ni_2O_7$. In our analysis, we have assumed that superconductivity, if any, occurs in the tetragonal structure phase. We speculate that other orders such as the charge density wave is more favored for lower symmetries, but such a competition between superconductivity and other orders is beyond the scope of the present paper, and serves as an interesting future issue.

We have also examined our theoretical analysis by performing experimental studies using our polycrystalline samples of $La_3Ni_2O_{7.01}$ and $La_4Ni_3O_{9.99}$. The superconducting transition of $La_3Ni_2O_{7.01}$ has been confirmed by a drop in the electrical resistance, as well as the magnetic field dependence of the resistance. We have observed a maximum onset T_c of 67.0 K at a pressure of 26.5 GPa. Similar temperature and magnetic field dependencies of the resistance have been observed also for $La_4Ni_3O_{9.99}$ under high pressure, where a drop in the resistance is observed at lower temperatures compared to $La_3Ni_2O_{7.01}$. Given the theoretical expectation,
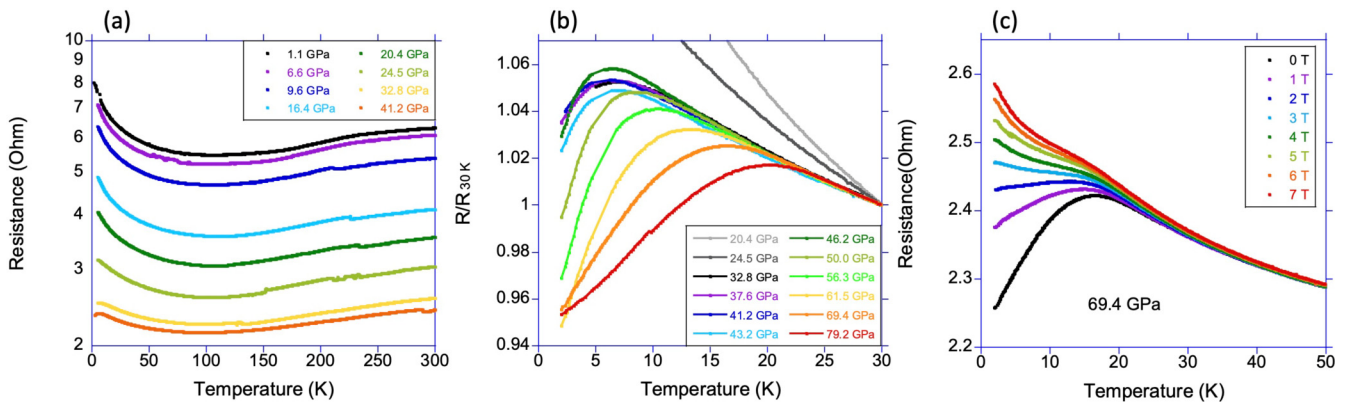

FIG. 6. Temperature dependence of the electrical resistance of $La_4Ni_3O_{9.99}$ (a) under several pressures from 1.1 to 41.2 GPa, (b) normalized at 30 K under 20.4–79.2 GPa, (c) under magnetic fields from 0 to 7 T at 69.4 GPa.

the reduction in the resistance can most likely be attributed to the occurrence of superconductivity in $La_4Ni_3O_{9.99}$, although we believe that further studies are necessary for a complete confirmation. The onset T_c, defined as the temperature at which the resistance deviates from a linear behavior, increases with pressure up to 23 K at 79.2 GPa, which is the opposite of what is observed for $La_3Ni_2O_{7.01}$. Understanding the origin of this difference between the two materials also serves as an interesting future study.

Recently, we became aware of an experimental study on polycrystalline samples [102]. The temperature and magnetic field dependencies of the resistance in $La_3Ni_2O_7$ observed there are quite similar to our results on $La_3Ni_2O_{7.01}$, while superconductivity is not observed in $La_4Ni_3O_{10}$ under the pressure of up to 50 GPa. Recently, there appeared three studies that suggest occurrence of superconductivity in $La_4Ni_3O_{10}$ under pressure. In Ref. [103], results simi-lar to ours were obtained for polycrystalline samples. In Refs. [104,105], single crystals were studied, and more clear drops of resistance were obtained at around 20–25 K at high pressures.

[1] F. D. M. Haldane, Phys. Rev. Lett. **50**, 1153 (1983).

[2] H. J. Schulz, Phys. Rev. B **34**, 6372 (1986).

[3] R. de Moriond, J. Tran, and G. Montambaux, *Correlated Fermions and Transport in Mesoscopic Systems: Proceedings of the XXXIst Rencontres de Moriond*, Series: Moriond Condensed Matter Physics (Atlantica Séguier Frontières, Les Arcs, Savoie, France, 1996), Vol. 90.

[4] E. Dagotto, J. Riera, and D. Scalapino, Phys. Rev. B **45**, 5744 (1992).

[5] T. M. Rice, S. Gopalan, and M. Sigrist, Europhys. Lett. **23**, 445 (1993).

[6] For a review, see E. Dagotto and T. M. Rice, Science **271**, 618 (1996), and references therein.

[7] M. Uehara, T. Nagata, J. Akimitsu, H. Takahashi, N. Môri, and K. Kinoshita, J. Phys. Soc. Jpn. **65**, 2764 (1996).

[8] T. Kimura, K. Kuroki, and H. Aoki, Phys. Rev. B **54**, R9608(R) (1996).

[9] E. Arrigoni, Phys. Lett. A **215**, 91 (1996).

[10] E. Arrigoni, Phys. Status Solidi B **195**, 425 (1996).

[11] H.-H. Lin, L. Balents, and M. P. A. Fisher, Phys. Rev. B **56**, 6569 (1997).

[12] N. Bulut, D. J. Scalapino, and R. T. Scalettar, Phys. Rev. B **45**, 5577 (1992).

[13] K. Kuroki, T. Kimura, and R. Arita, Phys. Rev. B **66**, 184508 (2002).

[14] T. A. Maier and D. J. Scalapino, Phys. Rev. B **84**, 180513(R) (2011).

[15] V. Mishra, D. J. Scalapino, and T. A. Maier, Sci. Rep. **6**, 32078 (2016).

[16] M. Nakata, D. Ogura, H. Usui, and K. Kuroki, Phys. Rev. B **95**, 214509 (2017).

[17] T. A. Maier, V. Mishra, G. Balduzzi, and D. J. Scalapino, Phys. Rev. B **99**, 140504(R) (2019).

[18] S. Karakuzu, S. Johnston, and T. A. Maier, Phys. Rev. B **104**, 245109 (2021).

[19] K. Matsumoto, D. Ogura, and K. Kuroki, J. Phys. Soc. Jpn. **89**, 044709 (2020).

[20] D. Kato and K. Kuroki, Phys. Rev. Res. **2**, 023156 (2020).

[21] H. Sun, M. Huo, X. Hu, J. Li, Z. Liu, Y. Han, L. Tang, Z. Mao, P. Yang, B. Wang, J. Cheng, D.-X. Yao, G.-M. Zhang, and M. Wang, Nature (London) **621**, 493 (2023).

[22] Z. Liu, M. Huo, J. Li, Q. Li, Y. Liu, Y. Dai, X. Zhou, J. Hao, Y. Lu, M. Wang, and H.-H. Wen, arXiv:2307.02950.

[23] J. Hou, P. T. Yang, Z. Y. Liu, J. Y. Li, P. F. Shan, L. Ma, G. Wang, N. N. Wang, H. Z. Guo, J. P. Sun, Y. Uwatoko, M. Wang, G.-M. Zhang, B. S. Wang, and J.-G. Cheng, Chin. Phys. Lett. **40**, 117302, (2023).

[24] Y. Zhang, D. Su, Y. Huang, H. Sun, M. Huo, Z. Shan, K. Ye, Z. Yang, R. Li, M. Smidman, M. Wang, L. Jiao, and H. Yuan, arXiv:2307.14819.

[25] J. Yang, H. Sun, X. Hu, Y. Xie, T. Miao, H. Luo, H. Chen, B. Liang, W. Zhu, G. Qu, C.-Q. Chen, M. Huo, Y. Huang, S. Zhang, F. Zhang, F. Yang, Z. Wang, Q. Peng, H. Mao, G. Liu *et al.*, arXiv:2309.01148.

[26] Y. Shen, M. Qin, and G.-M. Zhang, Chi. Phys. Lett. **40**, 127401 (2023).

[27] Q.-G. Yang, D. Wang, and Q.-H. Wang, Phys. Rev. B **108**, L140505 (2023).

[28] V. Christiansson, F. Petocchi, and P. Werner, Phys. Rev. Lett. **131**, 206501 (2023).

[29] W. Wú, Z. Luo, D.-X. Yao, and M. Wang, Sci. China Phys. Mech. Astron. **67**, 117402 (2024).

[30] Z. Liao, L. Chen, G. Duan, Y. Wang, C. Liu, R. Yu, and Q. Si, arXiv:2307.16697.

[31] X.-Z. Qu, D.-W. Qu, J. Chen, C. Wu, F. Yang, W. Li, and G. Su, Phys. Rev. Lett. **132**, 036502 (2024).

[32] H. Oh and Y.-H. Zhang, Phys. Rev. B **108**, 174511 (2023).

[33] Z. Luo, X. Hu, M. Wang, W. Wú, and D.-X. Yao, Phys. Rev. Lett. **131**, 126001 (2023).

[34] Y.-B. Liu, J.-W. Mei, F. Ye, W.-Q. Chen, and F. Yang, Phys. Rev. Lett. **131**, 236002 (2023).

[35] Y. Cao and Y.-f. Yang, Phys. Rev. B **109**, L081105 (2024).

[36] C. Lu, Z. Pan, F. Yang, and C. Wu, Phys. Rev. Lett. **132**, 146002 (2024).

[37] X. Chen, P. Jiang, J. Li, Z. Zhong, and Y. Lu, arXiv:2307.07154.

[38] Y. Zhang, L.-F. Lin, A. Moreo, and E. Dagotto, Phys. Rev. B **108**, L180510 (2023).

[39] Y. Zhang, L.-F. Lin, A. Moreo, T. A. Maier, and E. Dagotto, Nat. Commun. **15**, 2470 (2024).

[40] F. Lechermann, J. Gondolf, S. Botzel, and I. M. Eremin, Phys. Rev. B **108**, L201121 (2023).

[41] Y.-F. Yang, G.-M. Zhang, and F.-C. Zhang, Phys. Rev. B **108**, L201108 (2023).

[42] K. Jiang, Z. Wang, and F.-C. Zhang, Chin. Phys. Lett. **41**, 017402 (2024).

[43] Y. Gu, C. Le, Z. Yang, X. Wu, and J. Hu, arXiv:2306.07275.

[44] Z. Pan, C. Lu, F. Yang, and C. Wu, arXiv:2309.06173.

[45] J.-X. Zhang, H.-K. Zhang, Y.-Z. You, and Z.-Y. Weng, arXiv:2309.05726.

[46] Z. Luo, B. Lv, M. Wang, W. Wú, and D.-X. Yao, arXiv:2308.16564.

[47] R. Jiang, J. Hou, Z. Fan, Z.-J. Lang, and W. Ku, Phys. Rev. Lett. **132**, 126503 (2024).

[48] D.-C. Lu, M. Li, Z.-Y. Zeng, W. Hou, J. Wang, F. Yang, and Y.-Z. You, arXiv:2308.11195.

[49] Y.-H. Tian, Y. Chen, J.-M. Wang, R.-Q. He, and Z.-Y. Lu, arXiv:2308.09698.

[50] Q. Qin and Y.-F. Yang, Phys. Rev. B **108**, L140504 (2023).

[51] J. Huang, Z. D. Wang, and T. Zhou, Phys. Rev. B **108**, 174501 (2023).

[52] Y. Zhang, L.-F. Lin, A. Moreo, T. A. Maier, and E. Dagotto, Phys. Rev. B **108**, 165141 (2023).

[53] H. Lange, L. Homeier, E. Demler, U. Schollwöck, A. Bohrdt, and F. Grusdt, arXiv:2309.13040.

[54] B. Geisler, J. J. Hamlin, G. R. Stewart, R. G. Hennig, and P. Hirschfeld, arXiv:2309.15078.

[55] H. Sakakibara, N. Kitamine, M. Ochi, and K. Kuroki, Phys. Rev. Lett. **132**, 106002 (2024).

[56] J. P. Perdew, A. Ruzsinszky, G. I. Csonka, O. A. Vydrov, G. E. Scuseria, L. A. Constantin, X. Zhou, and K. Burke, Phys. Rev. Lett. **100**, 136406 (2008).

[57] G. Kresse and D. Joubert, Phys. Rev. B **59**, 1758 (1999).

[58] G. Kresse and J. Hafner, Phys. Rev. B **47**, 558 (1993).

[59] G. Kresse and J. Hafner, Phys. Rev. B **49**, 14251 (1994).

[60] G. Kresse and J. Furthmüller, Comput. Mater. Sci. **6**, 15 (1996).

[61] G. Kresse and J. Furthmüller, Phys. Rev. B **54**, 11169 (1996).

[62] A. Togo and I. Tanaka, Scr. Mater. **108**, 1 (2015).

[63] N. Marzari and D. Vanderbilt, Phys. Rev. B **56**, 12847 (1997).

[64] I. Souza, N. Marzari, and D. Vanderbilt, Phys. Rev. B **65**, 035109 (2001).

[65] G. Pizzi, V. Vitale, R. Arita, S. Blügel, F. Freimuth, G. Géranton, M. Gibertini, D. Gresch, C. Johnson, T. Koretsune *et al.*, J. Phys.: Cond. Matter **32**, 165902 (2020).

[66] N. E. Bickers, D. J. Scalapino, and S. R. White, Phys. Rev. Lett. **62**, 961 (1989).

[67] N. E. Bickers and S. R. White, Phys. Rev. B **43**, 8044 (1991).

[68] For La$_3$Ni$_2$O$_7$, we also performed FLEX calculation adopting a more realistic set of interaction values evaluated by constrained-RPA [28], and obtained similar results.

[69] A. I. Lichtenstein and M. I. Katsnelson, Phys. Rev. B **57**, 6884 (1998).

[70] K. Yada and H. Kontani, J. Phys. Soc. Jpn. **74**, 2161 (2005).

[71] M. Mochizuki, Y. Yanase, and M. Ogata, Phys. Rev. Lett. **94**, 147005 (2005).

[72] H. Ikeda, R. Arita, and J. Kuneš, Phys. Rev. B **81**, 054502 (2010).

[73] M. Kato, M. Nakanishi, T. Miyano, T. Shimizu, M. Kakihana, K. Yoshimura, and K. Kosuge, J. Solid State Chem. **139**, 266 (1998).

[74] C. D. Ling, D. N. Argyriou, G. Wu, and J. Neumeier, J. Solid State Chem. **152**, 517 (2000).

[75] H. Sakurai *et al.* (unpublished).

[76] R. Matsumoto, Y. Sasama, M. Fujioka, T. Irifune, M. Tanaka, T. Yamaguchi, H. Takeya, and Y. Takano, Rev. Sci. Instrum. **87**, 076103 (2016).

[77] R. Matsumoto, A. Yamashita, H. Hara, T. Irifune, S. Adachi, H. Takeya, and Y. Takano, Appl. Phys. Express **11**, 053101 (2018).

[78] G. J. Piermarini, S. Block, J. D. Barnett, and R. A. Forman, J. Appl. Phys. **46**, 2774 (1975).

[79] Y. Akahama and H. Kawamura, J. Appl. Phys. **96**, 3748 (2004).

[80] R. Matsumoto, Z. Hou, M. Nagao, S. Adachi, H. Hara, H. Tanaka, K. Nakamura, R. Murakami, S. Yamamoto, H. Takeya, T. Irifune, K. Terakura, and Y. Takano, Sci. Technol. Adv. Mater. **19**, 909 (2018).

[81] R. Matsumoto, T. Irifune, M. Tanaka, H. Takeya, and Y. Takano, Jpn. J. Appl. Phys. **56**, 05FC01 (2017).

[82] K. Momma and F. Izumi, J. Appl. Crystallogr. **44**, 1272 (2011).

[83] Z. Zhang and M. Greenblatt, J. Solid State Chem. **117**, 236 (1995).

[84] J. Zhang, H. Zheng, Y.-S. Chen, Y. Ren, M. Yonemura, A. Huq, and J. F. Mitchell, Phys. Rev. Mater. **4**, 083402 (2020).

[85] V. Voronin, I. Berger, V. Cherepanov, L. Gavrilova, A. Petrov, A. Ancharov, B. Tolochko, and S. Nikitenko, Nucl. Instrum. Methods Phys. Res., Sect. A **470**, 202 (2001); Proceedings of the 13th National Synchrotron Radiation Conference.

[86] M. U. Nagell, S. Kumar, M. H. Sørby, H. Fjellvåg, and A. O. Sjåstad, Phase Trans. **88**, 979 (2015).

[87] S. Kumar, Ø. Fjellvåg, A. O. Sjåstad, and H. Fjellvåg, J. Magn. Magn. Mater. **496**, 165915 (2020).

[88] M. Periyasamy, L. Patra, Ø. S. Fjellvåg, P. Ravindran, M. H. Sørby, S. Kumar, A. O. Sjåstad, and H. Fjellvåg, ACS Appl. Electron. Mater. **3**, 2671 (2021).

[89] A. Olafsen, H. Fjellvåg, and B. C. Hauback, J. Solid State Chem. **151**, 46 (2000).

[90] B.-Z. Li, C. Wang, P. T. Yang, J. P. Sun, Y.-B. Liu, J. Wu, Z. Ren, J.-G. Cheng, G.-M. Zhang, and G.-H. Cao, Phys. Rev. B **101**, 195142 (2020).

[91] S. Huangfu, X. Zhang, and A. Schilling, Phys. Rev. Res. **2**, 033247 (2020).

[92] S. Huangfu, G. D. Jakub, X. Zhang, O. Blacque, P. Puphal, E. Pomjakushina, F. O. von Rohr, and A. Schilling, Phys. Rev. B **101**, 104104 (2020).

[93] H. Li, X. Zhou, T. Nummy, J. Zhang, V. Pardo, W. E. Pickett, J. F. Mitchell, and D. S. Dessau, Nat. Commun. **8**, 704 (2017).

[94] D. Puggioni and J. M. Rondinelli, Phys. Rev. B **97**, 115116 (2018).

[95] H. Sakakibara, H. Usui, K. Kuroki, R. Arita, and H. Aoki, Phys. Rev. Lett. **105**, 057003 (2010).

[96] H. Sakakibara, H. Usui, K. Kuroki, R. Arita, and H. Aoki, Phys. Rev. B **85**, 064501 (2012).

[97] H. Sakakibara, K. Suzuki, H. Usui, S. Miyao, I. Maruyama, K. Kusakabe, R. Arita, H. Aoki, and K. Kuroki, Phys. Rev. B **89**, 224505 (2014).

[98] Similar bonding, nonbonding, and antibonding $d_{3z^2-r^2}$ bands were obtained in a band-structure calculation study for $La_4Ni_3O_{10}$ at ambient pressure [99].

[99] M.-C. Jung, J. Kapeghian, C. Hanson, B. Pamuk, and A. S. Botana, Phys. Rev. B **105**, 085150 (2022).

[100] For a brief summary on the effect of incipient bands in spin-fluctuation-mediated superconductivity, see N. Kitamine *et al.*, arXiv:2308.12750.

[101] S. Taniguchi, T. Nishikawa, Y. Yasui, Y. Kobayashi, J. Takeda, S.-i. Shamoto, and M. Sato, J. Phys. Soc. Jpn. **64**, 1644 (1995).

[102] M. Zhang, C. Pei, Q. Wang, Y. Zhao, C. Li, W. Cao, S. Zhu, J. Wu, and Y. Qi, J. Mater. Sci. Technol. **185**, 147 (2024).

[103] Q. Li, Y.-J. Zhang, Z.-N. Xiang, Y. Zhang, X. Zhu, and H.-H. Wen, Chinese Phys. Lett. **41**, 017401 (2024).

[104] M. Zhang, C. Pei, X. Du, Y. Cao, J. W. Qi Wang, Y. Li, Y. Zhao, C. Li, W. Cao, S. Zhu, Q. Zhang, N. Yu, P. Cheng, J. Zhao, Y. Chen, H. Guo, L. Yang, and Y. Qi, arXiv:2311.07423.

[105] Y. Zhu, E. Zhang, B. Pan, X. Chen, D. Peng, L. Chen, H. Ren, F. Liu, N. Li, Z. Xing, J. Han, J. Wang, D. Jia, H. Wo, Y. Gu, Y. Gu, L. Ji, W. Wang, H. Gou, Y. Shen *et al.*, arXiv:2311.07353.